ENVIRONMENTAL RESEARCH
LETTERS

LETTER

Arctic coastal hazard assessment considering permafrost thaw subsidence, coastal erosion, and flooding

Ziyi Wang[1,*], **Ming Xiao**[2], **Dmitry Nicolsky**[3], **Vladimir Romanovsky**[4,5], **Christopher McComb**[6] and **Louise Farquharson**[7]

[1] Graduate Student, Department of Civil and Environmental Engineering, The Pennsylvania State University, University Park, PA 16802, United States of America
[2] Professor, Department of Civil and Environmental Engineering, The Pennsylvania State University, University Park, PA 16802, United States of America
[3] Research Associate Professor, Geophysical Institute, University of Alaska Fairbanks, Fairbanks, AK 99775, United States of America
[4] Professor Emeritus, Geophysical Institute, University of Alaska Fairbanks, Fairbanks, AK 99775, United States of America
[5] Lead Scientist, Tumen State University, Tumen, Russia
[6] Associate Professor, Mechanical Engineering, Carnegie Mellon University, Pittsburgh, PA 15213, United States of America
[7] Research Assistant Professor, Geophysical Institute, University of Alaska Fairbanks, Fairbanks, AK 99775, United States of America
[*] Author to whom any correspondence should be addressed.

E-mail: ziyiwang@psu.edu

Keywords: coastal hazards, thaw subsidence, hazard assessment, permafrost, Northern Alaska

Supplementary material for this article is available online

OPEN ACCESS

RECEIVED
7 May 2023

REVISED
21 August 2023

ACCEPTED FOR PUBLICATION
29 August 2023

PUBLISHED
14 September 2023

Abstract

The thawing of permafrost in the Arctic has led to an increase in coastal land loss, flooding, and ground subsidence, seriously threatening civil infrastructure and coastal communities. However, a lack of tools for synthetic hazard assessment of the Arctic coast has hindered effective response measures. We developed a holistic framework, the Arctic Coastal Hazard Index (ACHI), to assess the vulnerability of Arctic coasts to permafrost thawing, coastal erosion, and coastal flooding. We quantified the coastal permafrost thaw potential (PTP) through regional assessment of thaw subsidence using ground settlement index. The calculations of the ground settlement index involve utilizing projections of permafrost conditions, including future regional mean annual ground temperature, active layer thickness, and talik thickness. The predicted thaw subsidence was validated through a comparison with observed long-term subsidence data. The ACHI incorporates the PTP into seven physical and ecological variables for coastal hazard assessment: shoreline type, habitat, relief, wind exposure, wave exposure, surge potential, and sea-level rise. The coastal hazard assessment was conducted for each 1 km^2 coastline of North Slope Borough, Alaska in the 2060s under the Representative Concentration Pathway 4.5 and 8.5 forcing scenarios. The areas that are prone to coastal hazards were identified by mapping the distribution pattern of the ACHI. The calculated coastal hazards potential was subjected to validation by comparing it with the observed and historical long-term coastal erosion mean rates. This framework for Arctic coastal assessment may assist policy and decision-making for adaptation, mitigation strategies, and civil infrastructure planning.

1. Introduction

The Arctic is experiencing significant changes and warming up to four times faster than the rate at lower latitudes (Rantanen *et al* 2022). An increase in air temperature leads to permafrost thaw and ground ice melt, which can lead to talik formation, thermokarst development, and associated ponding. Taliks are defined as perennially unfrozen zones above or within the permafrost (Ferrians *et al* 1969). In coastal areas, permafrost thaw, talik formation, and thermokarst processes can contribute to coastal erosion, as thawed sediments are more easily eroded than frozen ones.

Ocean wave dynamics also play an important role in coastal erosion in the Arctic. During calm conditions, waves can thermally erode frozen bluffs, whereas extreme storm surges and surface ocean

waves mechanically increase the vulnerability of the Arctic coast to erosion, leading to flooding and enhanced ground thawing in flooded areas (Irrgang *et al* 2022). The decline of sea-ice extent and duration increases the exposure to storms, enhancing Arctic wave- and storm-driven erosion. Projection suggests that sea ice will continue to decline as stormy conditions overlap more frequently with the open water sea (Barnhart *et al* 2016, Crawford *et al* 2021). Consequently, Arctic coastal hazards are expected to increase over the coming decades. Predicting the natural hazards of Arctic coasts for civil infrastructure planning and understanding society's capacity to adapt and transform are crucial for effectively preparing for an uncertain future.

Several assessment methods have been developed to evaluate and visualize the hazard potential associated with permafrost thaw subsidence, coastal erosion, and flooding. In thaw subsidence assessment, settlement (Nelson *et al* 2001) and bearing capacity (Streletskiy *et al* 2012) indices are the two primary approaches. Other methods related to subsidence assessment include the flow-diagram-based risk zonation index (Daanen *et al* 2011) and the analytical hierarchy process-based index (Hong *et al* 2014). For the evaluation of coastal erosion and flooding, Gornitz (1994) developed a Coastal Vulnerability Index that considers six variables: geomorphology, coastal slope, rate of relative sea-level rise, shoreline erosion, mean tide range, and mean wave height. Jaskólski *et al* (2018) applied this Coastal Vulnerability Index to assess high Arctic coastal vulnerability specifically in Longyearbyen, Svalbard. Arkema *et al* (2013) calculated a coastal hazard index (HI) for Alaska coastlines, aiming to identify areas at risk of inundation and erosion. The coastal HI integrates seven variables: habitat characteristics, shoreline type, coastal relief, sea-level rise, wind, wave, and surge potential. Manson *et al* (2019) employed a coastal sensitivity index to evaluate the sensitivity of Canada's marine coasts to climate change impacts. Casas-Prat and Wang (2020) computed pan-Arctic coastal hazards, focusing on wave characteristics and using the Inundation Index and Erosion Index (Jiménez *et al* 2012). The Inundation Index and Erosion Index comprise three variables: wave height, peak wave period, and storm duration.

To date, the thaw subsidence indices do not include zones of talik formation where previously frozen ground is now thawed year-round. This exclusion might lead to an underestimation of thaw subsidence in the analysis (Wang *et al* 2023). The development of assessment methods for evaluating combined Arctic coastal hazards is relatively rare when compared to their widespread utilization in low-latitude coastal regions. Previous efforts have been made by developing or applying indicator-based methods (Gornitz *et al* 1994, Ford and Smith 2004) or an empirical model (Casas-Prat and Wang *et al* 2020, Nielsen *et al* 2022) to assess Arctic coastal hazard or vulnerability. However, permafrost thaw was not explicitly considered in these frameworks. No attempt was made to integrate permafrost thaw, coastal erosion, and coastal flooding into a synthetic hazard assessment of the Arctic coast. To fill this knowledge gap, this study conducted an integrated analysis of the coastal plains of Alaska's northernmost borough, North Slope Borough.

The objectives of this research are to (1) present a regional-scale permafrost thaw subsidence assessment for North Slope Borough, Alaska, (2) develop a holistic framework for Arctic coastal hazards assessment that considers permafrost thaw subsidence, coastal erosion, and flooding, and (3) identify coastal areas of North Slope Borough that are prone to the three types of hazards.

2. Methods

2.1. Study area

This research studies the coastal regions of the North Slope Borough in Alaska. Figure 1 depicts the location and four coastal communities. They are Utqiaġvik, Wainwright, Point Lay, and Kaktovik. Continuous permafrost (90%–100% of areas underlain by perennially frozen ground) underlies the North Slope Borough with a thickness ranging from 200 m to more than 600 m (Osterkamp and Payne 1981). The permafrost has moderate to high ground ice content, with some parts of the coastal lowlands reaching up to approximately 80% ground ice by volume (Kanevskiy *et al* 2013). Owing to the presence of ice-rich permafrost and low-lying tundra terrain, the landscapes in these villages are vulnerable to widespread thaw subsidence, coastal erosion, and coastal flooding.

2.2. Data

In our assessment of thaw subsidence hazard, we utilized the pre-existing ground ice map of northern Alaska developed by Jorgenson *et al* (2014). This map provides information on the distribution of massive ice volume within the upper five meters of permafrost. For reference, the ground ice map can be found in figure S1 in the supplementary materials of this study.

The input variables that were utilized for the assessment of coastal hazard, including habitat and shoreline type, were derived from the *ShoreZone* database (NOAA *ShoreZone*). Specific details regarding the assignment of exposure ranks for different shoreline types and habitat classes can be found in supplementary tables S1 and S2, respectively. The spatial distribution of shore-type exposure rankings is visualized in figure S2, while the visualized habitat classes are depicted in supplementary figure S3.

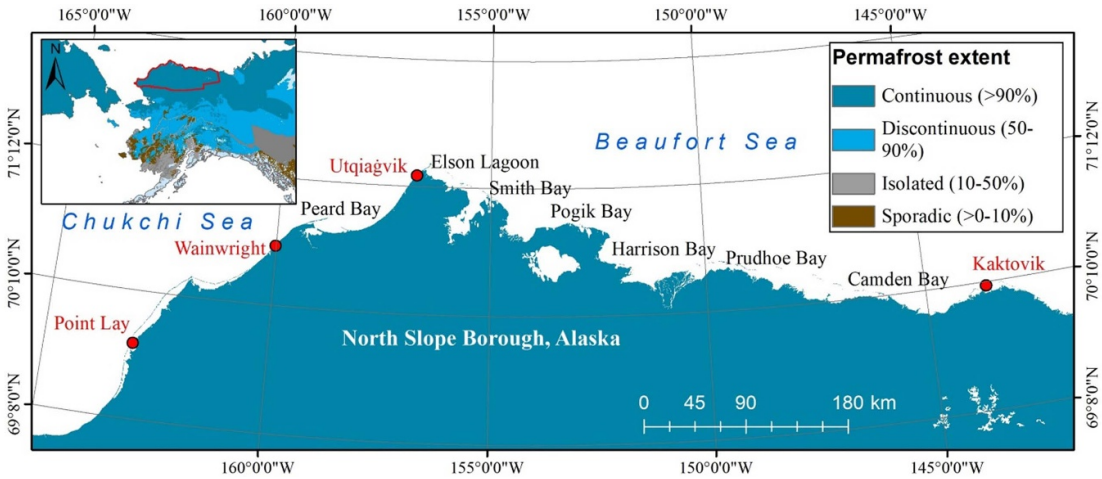

Figure 1. Locations of North Slope Borough, Alaska (covered with thick red line) and several coastal communities. The locations of coastal communities are indicated as red markers on the map of permafrost distributions. The Alaska permafrost map is adapted from Jorgenson *et al* (2008), and the permafrost map outside of Alaska is adapted from Brown *et al* (2002).

To determine the variable of coastal relief, we utilized an Arctic digital elevation model obtained from the Polar Geospatial Center (Porter *et al* 2018). For the exposure factors related to wind, wave, and surge potential, we utilized a compiled dataset derived from the WAVEWATCH III model spanning eight years (2008–2016) (NCP 2018).

To determine the sea level projections, we compiled data of mean projections of sea-level rise along the U.S. coastlines from the National Oceanic and Atmospheric Administration, as presented by Sweet *et al* (2022). These sea-level rise scenarios are related to the air temperature scenarios in this study, estimated based on the fifth phase of Coupled Model Intercomparison Project (CMICP5) models (Sweet *et al* 2022). For more detailed information regarding the classification and representation of the sea-level rise scenarios, please refer to figure S4.

2.3. General methodological framework

We integrate the index-based permafrost thaw potential (PTP) as an input variable into the Arctic coastal hazard assessment framework, as shown in figure 2. The conceptual framework consists of three steps: (1) assessment of permafrost conditions; (2) assessment of permafrost thaw subsidence; (3) assessment of Arctic coastal hazards.

First, *in-situ* field observations of mean annual ground temperature (MAGT) and active layer thickness (ALT), ground thermal properties, and environmental data serve as inputs for the Geophysical Institute's Permafrost Laboratory (GIPL)-2.0 model. MAGT, ALT and talik thickness projections from the GIPL model for the Representative Concentration Pathway (RCP) 4.5 and 8.4 are visualized in Geographical Information System (GIS)-based maps for the 2020s and the 2060s.

Second, using the input from thaw subsidence factors derived from existing ground ice maps (Jorgenson *et al* 2014) and the predicted MAGT, ALT, and talik thickness from the GIPL-2.0 model, the ground settlement index is quantified. The hazard indices are then used to delineate areas into five categories of PTP caused by the thawing of near-surface permafrost.

Third, the erosion and flooding factors combined with the gridded PTP from the second step constitute the input factors of the Arctic Coastal Hazard Index (ACHI). In this study, coastal hazard refers to thaw subsidence, flooding, and erosion caused by storms and permafrost thaw acting upon shorelines. Environmental risk encompasses the product of hazard occurrence and its potential societal consequences. ACHI is determined by incorporating thaw subsidence and erosion-flooding potential. In the following section, we describe each methodological step in detail.

2.4. Assessment of permafrost conditions

The GIPL-2.0 model simulates soil temperature dynamics and the depth of seasonal freezing and thawing by numerically solving 1D quasi-linear heat conductive equations with phase change (Marchenko *et al* 2008). The heat equation used in the GIPL model requires spatially distributed thermal conductivity, volumetric heat capacity, volumetric unfrozen water content, and volumetric latent heat of freezing and thawing as the input parameters (figure 2).

The permafrost conditions of North Slope Borough, Alaska were simulated using the GIPL-2.0 model by the co-authors (Nicolsky *et al* 2017). The simulation results are visualized on the website: https://permamap.gi.alaska.edu/. This study uses existing simulation data for hazard assessment.

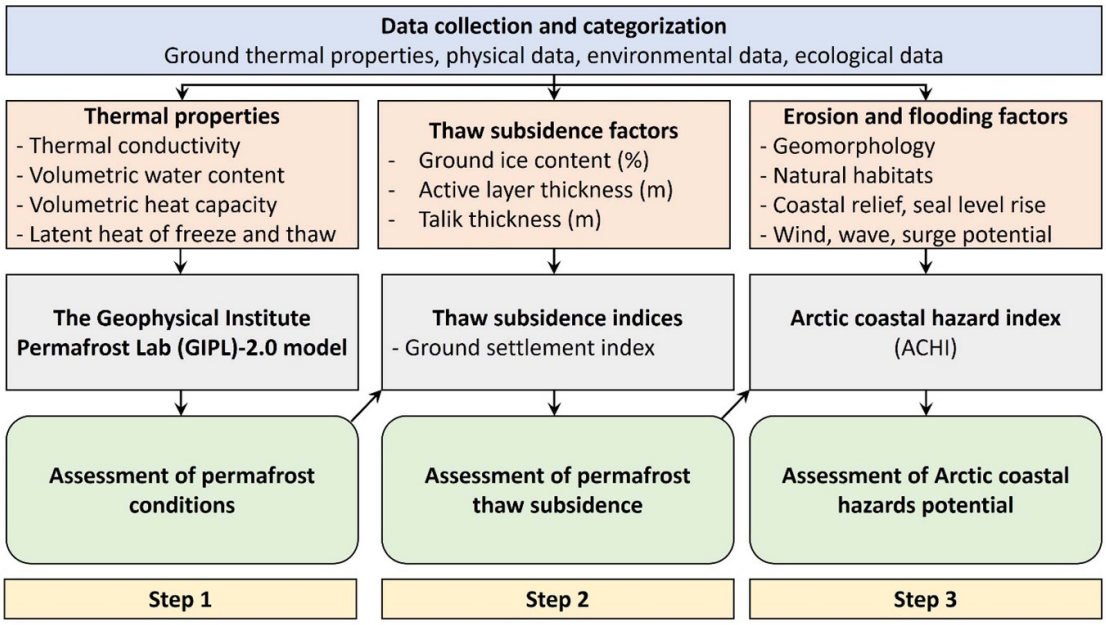

Figure 2. Schematic depiction of the integrated Arctic coastal hazard assessment framework.

Figures S5 and S6 show detailed information regarding the future permafrost conditions.

2.5. Assessment of permafrost thaw subsidence

We considered the role of taliks in the potential of permafrost thaw subsidence. Taliks in this study are defined by their physical state as unfrozen zones above or within permafrost. As mean annual air temperature increases, the depth of summer thaw begins to exceed the depth of winter freeze, resulting in the formation of sub-aerial taliks, as shown in figure 3. Farquharson *et al* (2022) used the concepts of potential freeze and potential thaw to determine the point in time when a sub-aerial supra-permafrost talik may begin to develop. The depth of potential freeze is characterized as the maximum extent of freeze reached by the end of a freezing period, assuming complete thawing of the subsurface material at the onset of freezing (Alexiades 1992). The depth of potential thaw is determined as the maximum depth of thaw attained by the conclusion of the thawing period, assuming complete subsurface freezing at the initiation of thawing (Alexiades 1992).

Nelson *et al* (2001) developed an approach to estimate the potential thaw subsidence of permafrost. The ground settlement index is constructed using data of changes in ALT and ground ice content. The calculation is based on the following assumptions: the liquid water produced by the thawing of ground ice drains away from the affected sites and thaw settlement is proportional to the thickness of the ice lost (Nelson *et al* 2002). The calculated thaw settlement signifies an upper bound estimate, as the computation assumes a transformation of the thawed permafrost into a non-porous state. In permafrost regions with sub-aerial taliks, talik thickness plays a crucial role in the occurrence of potential thaw settlement. Liquid water resulting from the talik formation drains away from the impacted sites. Solely considering changes in the ALT or the seasonally thawed/frozen layer may underestimate the maximum potential thaw settlement. To address this limitation, we propose an improved approach that incorporates changes in talik thickness to accurately estimate ground subsidence. The ground settlement index (I_s) is computed using equation (1):

$$I_s = \Delta Z_{\mathrm{ALT+TT}} \times V_{\mathrm{ice}} \tag{1}$$

where $\Delta Z_{\mathrm{ALT+TT}} = \Delta(Z_{\mathrm{ALT}} + Z_{\mathrm{TT}})$ is the relative changes in the combined ALT and talik thickness (m), as shown in figure 3, and V_{ice} is the volumetric ground ice content.

In order to achieve a detailed delineation of hazard conditions, we categorized the distribution of I_s for the 2060s in comparison to the 2020s using manual intervals. These intervals were determined based on the theoretical potential range of absolute thaw settlement (measured in meters). The five ranges for potential thaw settlement were defined as follows: 0.0–0.05 m, 0.05–0.15 m, 0.15–0.25 m, 0.25–0.35 m, and greater than 0.35 m. The upper bound of each range is inclusive. It is worth noting that the class breaks for both the RCP4.5 and RCP8.5 scenarios remained consistent to facilitate a comparison of temporal and spatial variations in hazard conditions.

2.6. Assessment of Arctic coastal hazards

We calculate the values of Arctic coastal hazards with future climate change scenarios through the coastal

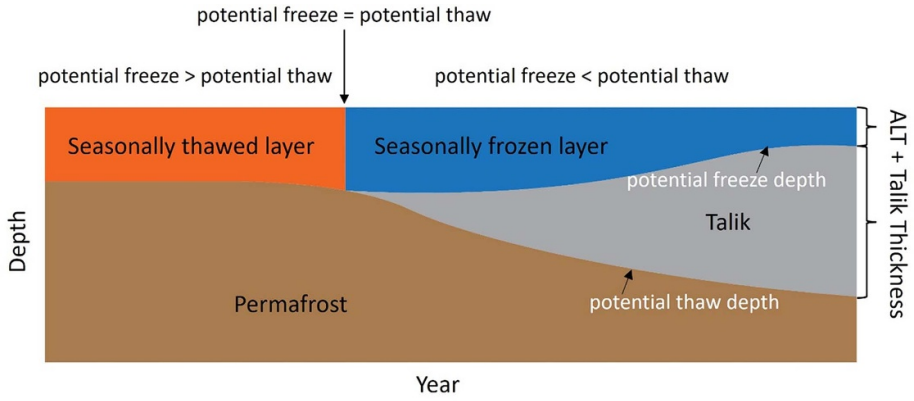

Figure 3. A schematic demonstrating the sub-aerial talik development and calculation of potential thaw settlement in regions with taliks.

vulnerability model within the open-source tool, InVEST (NCP 2018). The tool builds on previous analytical approaches and quantifies the impacts of storm surges on biophysical exposure (Gornitz 1994, Arkema *et al* 2013, Sharp *et al* 2014). The importance of the input factors is ranked from 1 (very low) to 5 (very high) for different hazard levels. The HI is calculated as the geometric mean of the seven constituent factors (equation (2)) (Arkema *et al* 2013):

$$\mathrm{HI} = (R_{\mathrm{Habitats}} R_{\mathrm{ShorelineType}} R_{\mathrm{Relief}} R_{\mathrm{Wind}} R_{\mathrm{Waves}} \times R_{\mathrm{SurgePotential}} R_{\mathrm{SLR}})^{1/7} \quad (2)$$

where R_{Habitats} refers to the habitat type, $R_{\mathrm{ShorelineType}}$ represents the geomorphology type, R_{Relief} represents the coastal relief (i.e. topography), R_{Wind} is the wind exposure, R_{Waves} is the wave exposure, $R_{\mathrm{SurgePotential}}$ is the surge potential, and R_{SLR} represents sea-level rise scenarios. Because each of the seven factors has a range of 1–5 and HI is an average value of these factors. HI has a range of 1–5. A detailed explanation of each class is provided in the supplementary materials.

The Arctic coastal setting is influenced by complex interaction mechanisms between thermal and mechanical drivers. The variability in Arctic Coastal Dynamics (ACD) results from coastal settings and environmental drivers. Arctic coastal settings are determined by the wave energy, coastal morphology, lithological characteristics (Wang *et al* 2022a, 2022b), and the ground thermal regime. Environmental drivers include air and water temperature, sea ice, wave climatology, storm intensity and timing, and sea-level changes (Irrgang *et al* 2022). When ice-rich permafrost bluffs are subjected to thawing due to MAGT increases, the volumetric land loss may be three times higher than that directly associated with coastal erosion (Lim *et al* 2020). We developed a composite ACHI based on equation (2), by including the permafrost thaw subsidence potential, as shown in equation (3):

$$\mathrm{ACHI} = \sqrt{HI \times R_{\mathrm{PTP}}} \quad (3)$$

where R_{PTP} represents the permafrost thaw potential (PTP).

R_{PTP} is derived from index-based permafrost thaw hazard maps from step 2 with a spatial resolution of 1 km. The complete coastline was partitioned into 10 376 segments, with a spatial resolution of 1 km × 1 km for each individual segment. Raster maps of the potential thaw settlement are used to calculate the PTP of each 1 km^2 shoreline area (i.e. the segment point). The five-class thaw subsidence hazard maps are first given a ranked number of 1, 2, 3, 4, or 5 representing low to high hazard potential. We calculate the average PTP within a radius of 3 km to decrease the uncertainty. The average PTP is then assigned to the nearest segment point to represent the shoreline PTP. The gridded shoreline PTP can be found in supplementary figure S7.

3. Results and discussion

3.1. Regional-scale projection of permafrost thaw subsidence potential

Two GIS-based thaw subsidence hazard maps were generated in this study, comparing the 2060s to the 2020s under two climate forcing scenarios, RCP4.5 and RCP8.5 (figure 4). The two hazard maps exhibit relatively consistent geographic variation. Regions with relatively higher potential for thaw subsidence are primarily concentrated along the west coast of the Beaufort Sea, the middle portion of the North Slope Borough, and low-latitude upland areas.

Under the RCP4.5 scenario, a significant portion of the Alaska coastal plain exhibits potential thaw settlement ranges between 0 and 5 cm from the 2020s to the 2060s. Some sections of the west Beaufort Sea coast show potential thaw subsidence ranges between 5 and 15 cm during the same time frame. On the other hand, under the RCP8.5 scenario, major parts

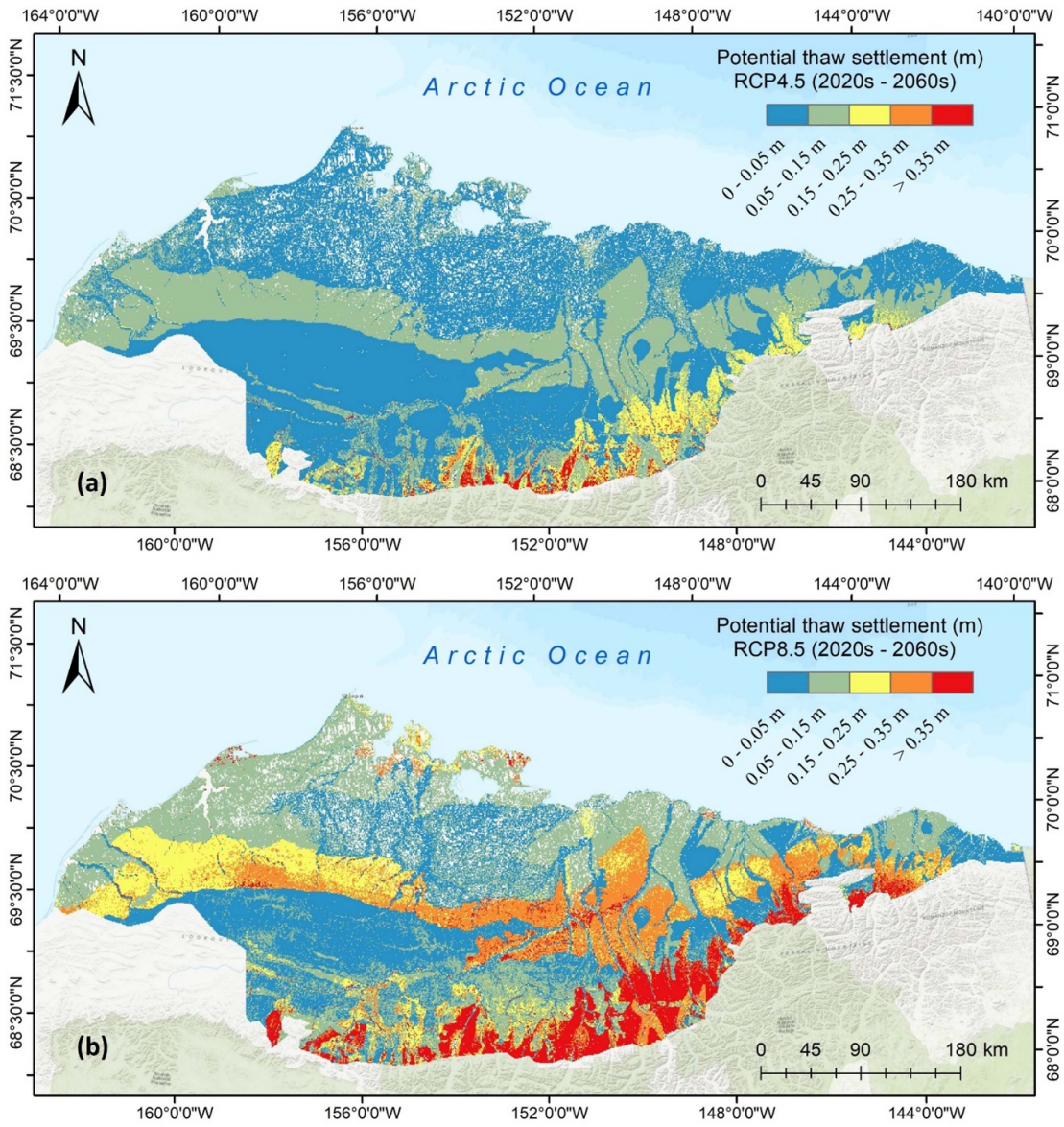

Figure 4. Maximum potential thaw settlement (m) for the 2060s compared against 2020s. (a) Predicted results using RCP4.5 climate forcing; (b) predicted results using RCP8.5 climate forcing.

of the Alaska coastal plain display potential thaw settlement ranges between 5 and 15 cm from the 2020s to the 2060s. Additionally, certain areas along the west Beaufort Sea coast exhibit potential thaw subsidence greater than 35 cm during this period.

The spatial patterns observed for thaw subsidence in our study align with the findings of a previous assessment conducted by Jorgenson *et al* (2014) regarding potential thaw settlement. Jorgenson *et al* (2014) developed a settlement map that primarily relied on the characterization of ground ice. We propose that the spatial patterns for potential thaw subsidence are primarily influenced by the presence and distribution of ground ice, which, in turn, is closely associated with cryolithology and Quaternary depositional environments.

3.2. Validation of permafrost thaw subsidence

In order to evaluate the efficacy of the ground settlement index in estimating thaw subsidence, a comparative analysis was conducted between our calculated estimates for potential thaw settlement and the observed surface subsidence in regions of Northern Alaska where permafrost is prevalent.

Figure 5(a) shows the prediction of potential thaw settlement along the Beaufort Sea coast using the ground settlement index. The calculated potential thaw settlement is for the 2060s compared to the 2020s under RCP8.5 forcing scenarios. The study region that is delineated by the dashed black line is situated in Prudhoe Bay region, positioned at the central portion of the Beaufort Sea coast. Figure 5(b) depicts the long-term subsidence rates in the study

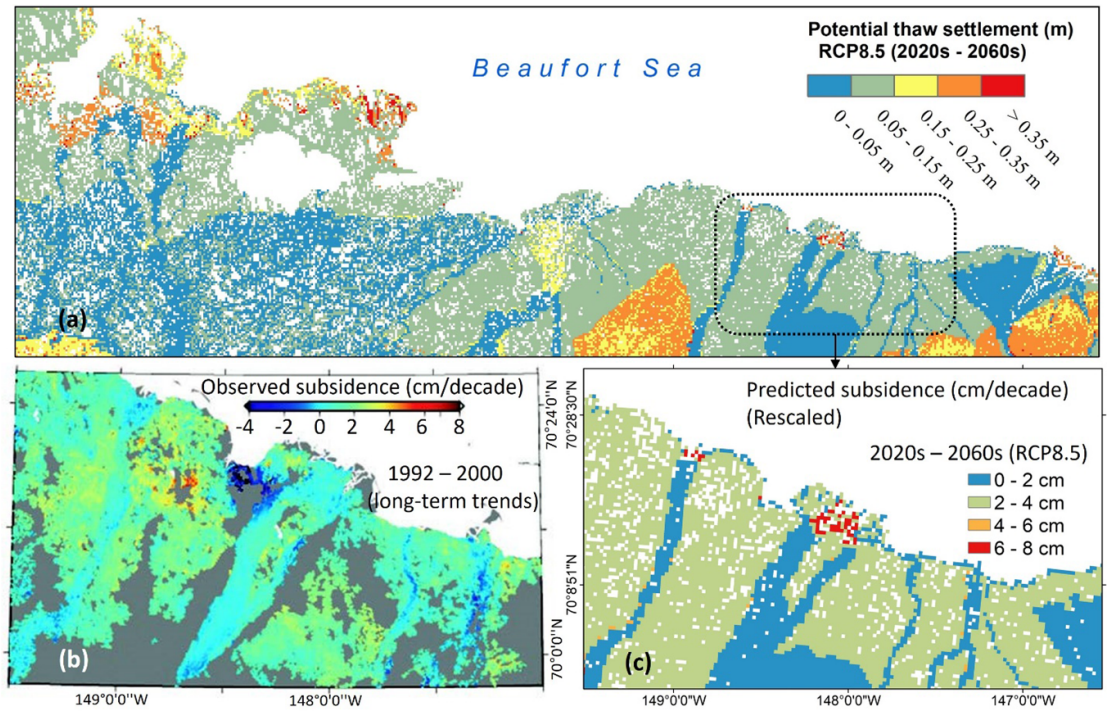

Figure 5. Spatial variability of predicted and observed thaw settlement (m). (a) Maximum potential thaw settlement using RCP8.5 climate forcing for the 2060s compared against 2020s; (b) observed long-term subsidence rates (cm/decade) between 1992 and 2000 using InSAR techniques (Liu *et al* 2010); Liu *et al* (2010) John Wiley & Sons. Copyright 2010 by the American Geophysical Union. (c) predicted subsidence rates (cm/decade) between 2020s and 2060s using ground settlement index.

region, spanning from 1992 to 2000, examined using Interferometric Synthetic Aperture Radar (InSAR) measurements. Figure 5(b) shows observed long-term trends in surface subsidence at rates of 1–4 cm per decade, as reported by Liu *et al* (2010). In figure 5(c), we have rescaled the predictions of regional settlement in centimeters per decade. According to figure 5(c), over 95% of the study region (calculated based on pixel numbers) exhibits a potential settlement ranging from 1 to 4 cm per decade. The projected values and distribution for thaw subsidence rates between 2020s and 2060s align with the long-term trends observed between 1992 and 2000.

3.3. Coastal hazards evaluation for North Slope Borough, Alaska

The distributions of the ACHI are classified into quartiles to represent different levels of coastal hazard scores. The quartiles are defined as follows: high (upper 25%, ranging between 3.5 and 5), moderate (50%–75%, ranging between 3.2 and 3.5), low (25%–50%, ranging between 2.8 and 3.2), and stable (lower 25%, ranging from 1 to 2.8); the upper bound of each range is inclusive. Figure 6 shows the predicted ACHI results of coastal hazard potential of North Slope Borough, Alaska by 2060s using RCP4.5 and 8.5 climate forcing. Both hazard maps demonstrate a relatively consistent geographic distribution of ACHI. Regions with relatively higher potential for coastal hazards are primarily concentrated along the west coast of the Beaufort Sea, including the coastline of Point Barrow, Smith Bay, and Pogik Bay. Additionally, the regions between Wainwright and Peard Bay also exhibit elevated levels of potential coastal hazards.

In the RCP4.5 scenario, the coastal areas spanning from Point Barrow to Pogik Bay primarily exhibit a coastal hazard potential ranging from low to moderate levels until the 2060s. However, under the RCP8.5 scenario, a significant portion of the same coastal region is characterized by a high potential for coastal hazards. Additionally, specific areas along the Wainwright, Point Lay, and Kaktovik coastline also demonstrate a notable high potential for coastal hazards, primarily due to high ground ice contents.

Regions characterized by a relatively higher potential for coastal hazards are driven primarily by cryolithology and Quaternary geology. Specifically, the higher potential for coastal hazards observed between Smith Bay and Pogik Bay can be attributed to several factors. Notably, the increased wind, wave, and surge potential in this region, along with the exposed shoreline type characterized by ice-rich silt, contribute significantly to the heightened hazard potential. Moreover, when considering permafrost thawing, it becomes evident that areas along the west Chukchi Sea with greater hazard potential are primarily influenced by permafrost thaw and the absence of protective features within their exposed habitat class.

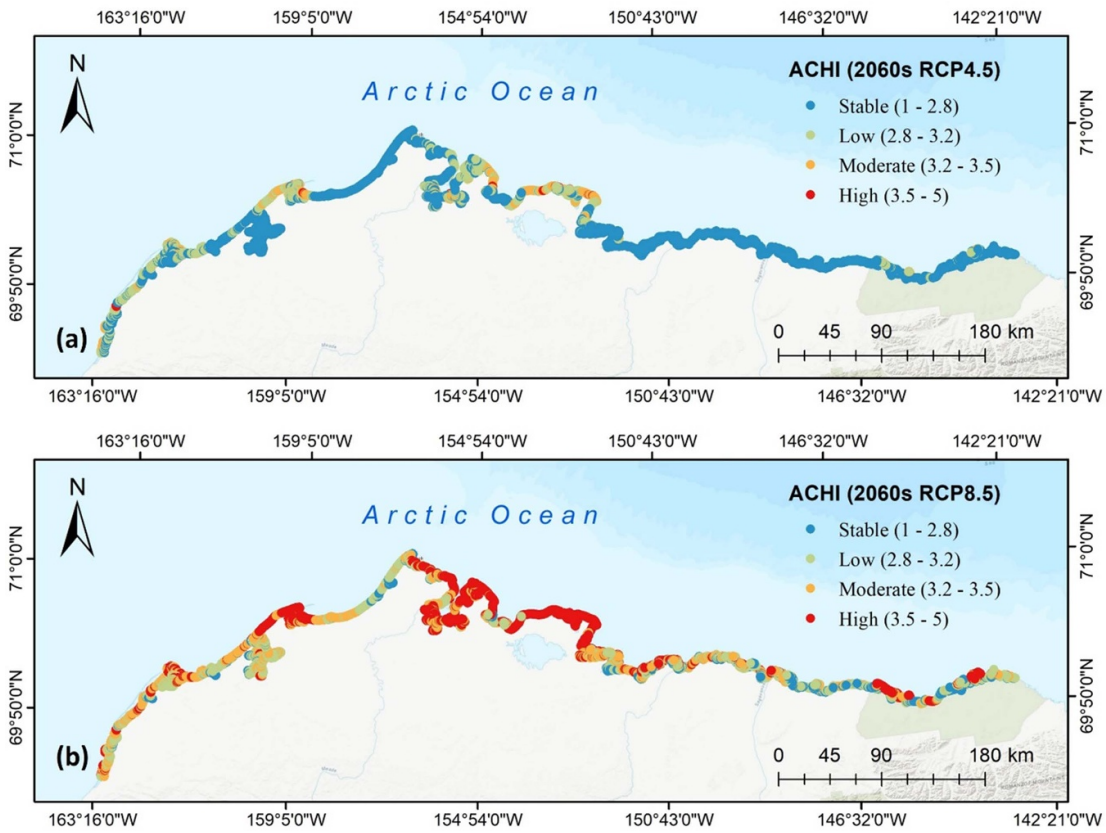

Figure 6. Predicted ACHI results of coastal hazard potential of North Slope Borough, Alaska by 2060s. (a) Using RCP4.5 climate forcing; (b) using RCP8.5 climate forcing.

3.4. Validation of Arctic coastal hazard potential

To assess the efficacy of ACHI in evaluating Arctic coastal hazard, we conducted a comparative analysis between the estimated coastal hazard potential based on RCP8.5 forcing scenario and the observed long-term coastal erosion mean rates obtained from the ACD database (Lantuit *et al* 2020) (figure 7(a)). We also considered the historical long-term rates of shoreline change reported by Gibbs *et al* (2017) (figure 7(b)). As shown in figures 7(a) and (b), the historical data were reclassified into four distinct classes, namely stable or aggrading, slow erosion (0–1 m per year), moderate erosion (1–2 m per year), and rapid erosion (>2 m per year). The projected ACHI results were then categorized into quartiles to represent varying levels of coastal hazard potential: stable (0%–25%), low (25%–50%), moderate (50%–75%), and high (>75%); the upper bound of each range is inclusive.

The spatial distribution of the predicted patterns by ACHI (figure 7(c)) demonstrated a strong agreement with both the observed and historical long-term coastal hazard data. Within the coastal region from Point Barrow to Pogik Bay, 92% of segments display a notable potential for moderate to high coastal hazards. This finding aligns with the historical data reported by Gibbs *et al* (2017) and Lantuit *et al* (2020), revealing nearly 90% and 86%, respectively. In other regions, such as the east and west Chukchi Sea coasts, as well as the central and eastern Beaufort coast, our projected values also align with the historical data, indicating a propensity for stable to moderate coastal hazards. It is worth noting that the regions between Wainwright and Peard Bay exhibit a high coastal hazard potential, primarily attributed to the increased likelihood of thaw settlement in these areas. The comparisons were drawn across different timelines: the historical data represent shoreline movement or erosion under past conditions, whereas the ACHI is designed to forecast future shoreline conditions.

3.5. Limitations of this study

The proposed framework has several limitations:

1) Crylithology is a key factor influencing the ACHI yet ground ice mapping to date has been conducted at a relatively coarse resolution. As such, for many regions, the ground ice volumes are not well constrained.
2) Similarly, vegetation cover, organic layer thickness, and lithology are essential in the ground thermal regime. Still, field-based observations are very sparse, which limits the accuracy of numerical modeling efforts.

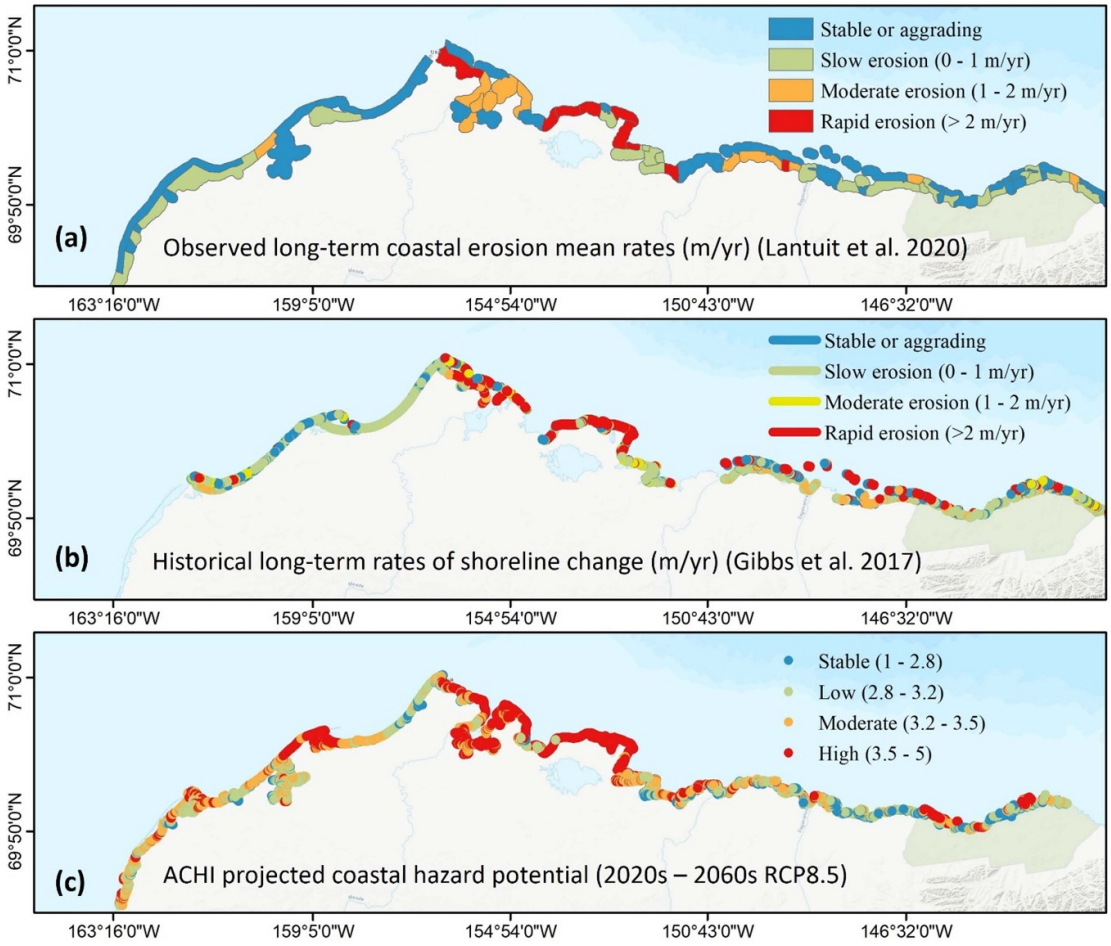

Figure 7. Historical and projected coastal hazard spatial variability. (a) Observed long-term coastal erosion mean rates from the ACD database (Lantuit *et al* 2020); (b) historical long-term rates of shoreline change (Gibbs *et al* 2017). (c) ACHI projected coastal hazard potential by 2060s using RCP8.5 climate forcing.

3) Decline in Arctic sea ice extent and increase in the open water period accelerate coastal erosion and impact biological productivity (Barnhart *et al* 2016). However, sea ice extent factors are not considered in the ACHI because of data deficiency.
4) The presence of barrier islands plays a role in reducing wave energy and protecting the coast from erosion (Irrgang *et al* 2022, Nederhoff *et al* 2022). However, the computation of wind and wave exposure did not consider the impact of barrier islands, which might lead to an overestimation of the exposure in protected regions. Furthermore, how barrier island morphology and movement may change with an increasingly longer open water season is very poorly understood (Moore *et al* 2014, Gibbs *et al* 2023).
5) The validation of predicted results has challenges due to the limited availability of field observations and ground-truthing data. Few long-term monitoring sites are situated along the Arctic coast.

4. Conclusions

This study developed the ACHI to comprehensively analyze Arctic coastal hazards by integrating thermal and mechanical drivers into a single spatial representation. To develop the ACHI, a large-scale permafrost thaw subsidence assessment is first conducted for North Slope Borough, Alaska. The assessment calculates the potential of maximum thaw settlement and determines the relative hazard ranking of PTP of those regions in 2060s compared to 2020s. The development of taliks is considered in the ground settlement index. The predicted values of thaw settlement demonstrate alignment with long-term observations of thaw subsidence in Northern Alaska.

The coastal PTP of the North Slope Borough is then gridded and assigned to the coastline segments as an input factor of the ACHI. The ACHI incorporates PTP with classified geomorphology, habitat, wind, wave, surge potential, coastal relief, and sea-level rise in coastal hazard assessment. The

ACHI provides a macro-picture of the North Slope Borough's heterogeneous coastal hazard potential at spatial scale of 1 km^2 under current and future climate change scenarios. The ACHI prediction shows that by the middle of this century, the areas categorized as high hazard are mainly distributed along the west Beaufort Sea coast, including Point Barrow, Smith Bay, and Pogik Bay. The predicted coastal hazard potential aligns with the observed and historical long-term coastal erosion mean rates.

Data availability statements

All data that support the findings of this study are included within the article (and any supplementary files).

Acknowledgments

Z W, M X, and C M were supported by the U.S. National Science Foundation (NSF) (Grant Number: RISE-1927718). M X was also supported by NSF (Grant Numbers: OISE-1927137, OPP-1945369). L F, V R and D N were supported by NSF (Grant Number: RISE-1927708).

Conflict of interest

The authors declare no competing interests.

ORCID iDs

Ziyi Wang https://orcid.org/0000-0003-3382-7576
Ming Xiao https://orcid.org/0000-0003-4791-0346
Vladimir Romanovsky https://orcid.org/0000-0002-9515-2087

References

Alexiades V 1992 *Mathematical Modeling of Melting and Freezing Processes* (CRC Press)
Arkema K K, Guannel G, Verutes G, Wood S A, Guerry A, Ruckelshaus M, Kareiva P, Lacayo M and Silver J M 2013 Coastal habitats shield people and property from sea-level rise and storms *Nat. Clim. Change* **3** 913–8
Barnhart K R, Miller C R, Overeem I and Kay J E 2016 Mapping the future expansion of Arctic open water *Nat. Clim. Change* **6** 280–5
Brown J B, Ferrians O J, Heginbottom J A and Melnikov E S 2002 Circum-Arctic map of permafrost and ground ice conditions, Version 2 *National Snow and Ice Data Center* (https://doi.org/10.7265/skbg-kf16)
Casas-Prat M and Wang X L 2020 Projections of extreme ocean waves in the Arctic and potential implications for coastal inundation and erosion *J. Geophys. Res. Oceans* **125** e2019JC015745
Crawford A, Stroeve J, Smith A and Jahn A 2021 Arctic open-water periods are projected to lengthen dramatically by 2100 *Commun. Earth Environ.* **2** 109
Daanen R P, Ingeman-Nielsen T, Marchenko S S, Romanovsky V E, Foged N, Stendel M, Christensen J H and Hornbech Svensen K 2011 Permafrost degradation risk zone assessment using simulation models *Cryosphere Discuss.* **5** 1021–53
Farquharson L M, Romanovsky V E, Kholodov A and Nicolsky D 2022 Sub-aerial talik formation observed across the discontinuous permafrost zone of Alaska *Nat. Geosci.* **15** 475–81
Ferrians O J, Kachadoorian R and Greene G W 1969 *Permafrost and Related Engineering Problems in Alaska* vol 678 (US Government Printing Office)
Ford J D and Smit B 2004 A framework for assessing the vulnerability of communities in the Canadian Arctic to risks associated with climate change *Arctic* **57** 389–400
Gibbs A E, Erikson L H and Hamilton A I 2023 Barrier islands and spits of northern Alaska: decadal scale morphological change *Coastal Sediments 2023: The Proc. Coastal Sediments 2023* pp 36–43
Gibbs A E, Ohman K A, Coppersmith R and Richmond B M 2017 *National Assessment of Shoreline Change: A GIS Compilation of Updated Vector Shorelines and Associated Shoreline Change Data for the North Coast of Alaska, U.S. Canadian Border to Icy Cape* (U.S. Geological Survey data release) (https://doi.org/10.5066/F72Z13N1)
Gornitz V M, Daniels R C, White T W and Birdwell K R 1994 The development of a coastal risk assessment database: vulnerability to sea-level rise in the US Southeast *J. Coast. Res.* **12** 327–38 (available at: www.jstor.org/stable/25735608)
Hong E, Perkins R and Trainor S 2014 Thaw settlement hazard of permafrost related to climate warming in Alaska *Arctic* **67** 93–103
Irrgang A M *et al* 2022 Drivers, dynamics and impacts of changing Arctic coasts *Nat. Rev. Earth Environ.* **3** 39–54
Jaskólski M W, Pawłowski Ł and Strzelecki M C 2018 High Arctic coasts at risk—the case study of coastal zone development and degradation associated with climate changes and multidirectional human impacts in Longyearbyen (Adventfjorden, Svalbard) *Land Degrad. Dev.* **29** 2514–24
Jiménez J A, Sancho-García A, Bosom E, Valdemoro H I and Guillén J 2012 Storm-induced damages along the Catalan coast (NW Mediterranean) during the period 1958–2008 *Geomorphology* **143** 24–33
Jorgenson M T, Kanevskiy M, Shur Y, Grunblatt J, Ping C L and Michaelson G 2014 *Permafrost database development, characterization, and mapping for northern Alaska* (available at: http://hdl.handle.net/11122/10373)
Jorgenson M T, Yoshikawa K, Kanevskiy M, Shur Y, Romanovsky V, Marchenko S, Grosse G, Brown J and Jones B 2008 Permafrost characteristics of Alaska *Proc. of the Ninth Int. Conf. on Permafrost (June)* vol 3 (University of Alaska) pp 121–2
Kanevskiy M, Shur Y, Jorgenson M T, Ping C L, Michaelson G J, Fortier D, Stephani E, Dillon M and Tumskoy V 2013 Ground ice in the upper permafrost of the Beaufort Sea coast of Alaska *Cold Reg. Sci. Technol.* **85** 56–70
Lantuit H *et al* 2020 The ACD classification of Arctic coasts (PANGAEA) (https://doi.org/10.1594/PANGAEA.919573)
Lim M, Whalen D, Martin J, Mann P J, Hayes S, Fraser P, Berry H B and Ouellette D 2020 Massive ice control on permafrost coast erosion and sensitivity *Geophys. Res. Lett.* **47** e2020GL087917
Liu L, Zhang T and Wahr J 2010 InSAR measurements of surface deformation over permafrost on the North Slope of Alaska *J. Geophys. Res. Earth Surf.* **115** F03023
Manson G K, Couture N J and James T S 2019 *CanCoast 2.0: data and indices to describe the sensitivity of Canada's marine coasts to changing climate* Open File 8551 (Geological Survey of Canada) (https://doi.org/10.4095/314669)
Marchenko S, Romanovsky V and Tipenko G 2008 Numerical modeling of spatial permafrost dynamics in Alaska *Proc. Ninth Int. Conf. on Permafrost (June)* vol 29 (Institute of Northern Engineering, University of Alaska Fairbanks) pp 1125–30
Moore L J, Patsch K, List J H and Williams S J 2014 The potential for sea-level-rise-induced barrier island loss: Insights from

the Chandeleur Islands, Louisiana, USA *Mar. Geol.* **355** 244–59
NCP 2018 Natural capital project: InVEST version 3.5.0 sample datasets (available at: http://data.naturalcapitalproject.org/invest-data) Accessed: 112-10-20182023
Nederhoff K, Erikson L, Engelstad A, Bieniek P and Kasper J 2022 The effect of changing sea ice on wave climate trends along Alaska's central Beaufort Sea coast *Cryosphere* **16** 1609–29
Nelson F E, Anisimov O A and Shiklomanov N I 2001 Subsidence risk from thawing permafrost *Nature* **410** 889–90
Nelson F E, Anisimov O A and Shiklomanov N I 2002 Climate change and hazard zonation in the circum-Arctic permafrost regions *Nat. Hazards* **26** 203–25
Nicolsky D J, Romanovsky V E, Panda S K, Marchenko S S and Muskett R R 2017 Applicability of the ecosystem type approach to model permafrost dynamics across the Alaska North Slope *J. Geophys. Res. Earth Surf.* **122** 50–75
Nielsen D M, Pieper P, Barkhordarian A, Overduin P, Ilyina T, Brovkin V, Baehr J and Dobrynin M 2022 Increase in Arctic coastal erosion and its sensitivity to warming in the twenty-first century *Nat. Clim. Change* **12** 263–70
NOAA 2023 Sea level and coastal flooding information (National Ocean Service Website) (available at: https://tidesandcurrents.noaa.gov/sea_level_info.html)
Osterkamp T E and Payne M W 1981 Estimates of permafrost thickness from well logs in northern Alaska *Cold Reg. Sci. Technol.* **5** 13–27
Porter C *et al* 2018 ArcticDEM *Harv. Dataverse* **1** 2018–30
Rantanen M, Karpechko A Y, Lipponen A, Nordling K, Hyvärinen O, Ruosteenoja K, Vihma T and Laaksonen A 2022 The Arctic has warmed nearly four times faster than the globe since 1979 *Commun. Earth Environ.* **3** 168
Sharp R *et al* 2014 *InVEST User's Guide* (The Natural Capital Project)
Streletskiy D A, Shiklomanov N I and Nelson F E 2012 Permafrost, infrastructure, and climate change: a GIS-based landscape approach to geotechnical modeling *Arct. Antarct. Alp. Res.* **44** 368–80
Sweet W V *et al* 2022 *Global and Regional Sea Level Rise Scenarios for the United States: Updated Mean Projections and Extreme Water Level Probabilities along US Coastlines* (National Oceanic and Atmospheric Administration)
Wang Z Y, Fang Y F, Feng W Q, Tian X J and Lin J F 2022a Comparative study on particle size effect of crushable granular soils through DEM simulations *Lithosphere* **2021** 1608454
Wang Z Y, Wang P, Yin Z Y and Wang R 2022b Micromechanical investigation of the particle size effect on the shear strength of uncrushable granular materials *Acta Geotech.* **17** 4277–96
Wang Z *et al* 2023 Arctic geohazard mapping tools for civil infrastructure planning: a systematic review *Cold Reg. Sci. Technol.* **214** 103969

Supplementary Materials

Arctic Coastal Hazard Assessment Considering Permafrost Thaw Subsidence, Coastal Erosion, and Flooding

Authors: Ziyi Wang[1], Ming Xiao[2], Dmitry Nicolsky[3], Vladimir Romanovsky[4], Christopher McComb[5], Louise Farquharson[6]

[1]Graduate Student, Department of Civil and Environmental Engineering, The Pennsylvania State University, University Park, PA 16802, United States of America. Email: ziyiwang@psu.edu.
[2]Professor, Department of Civil and Environmental Engineering, The Pennsylvania State University, University Park, PA 16802, United States of America. Email: mzx102@psu.edu.
[3]Research Associate Professor, Geophysical Institute, University of Alaska Fairbanks, Fairbanks, AK 99775, United States of America. Email: djnicolsky@alaska.edu.
[4]Professor Emeritus, Geophysical Institute, University of Alaska Fairbanks, Fairbanks, AK 99775, United States of America. Lead Scientist, Tumen State University, Tumen, Russia. Email: veromanovsky@alaska.edu.
[5]Associate Professor, Mechanical Engineering, Carnegie Mellon University, Pittsburgh, PA 15213, United States of America. Email: ccm@cmu.edu.
[6]Research Assistant Professor, Geophysical Institute, University of Alaska Fairbanks, Fairbanks, AK 99775, United States of America. Email: lmfarquharson@alaska.edu.

Corresponding author: ziyiwang@psu.edu; Department of Civil and Environmental Engineering, 212 Sackett Building, The Pennsylvania State University, University Park, PA 16802-1408.

1 Ground ice map

Figure S.1. shows the ground ice content distribution of North Slope Borough, Alaska; it is adapted from Jorgenson et al. (2014). The map was explicitly developed for northern Alaska based on the terrain-unit approach. Jorgenson et al. (2014) attributed the permafrost ice wedge polygon with dominant geomorphic units and characterized those units by compiling and analyzing in-situ field data. The ground ice map classified the ground ice volumes in permafrost into six categories: poorly known, <5%, 5-10%, 10-30%, 30-70%, and 10-80%. To calculate the maximum potential thaw subsidence, we use the upper value of each class: 0%, 5%, 10%, 30%, 70%, and 80%.

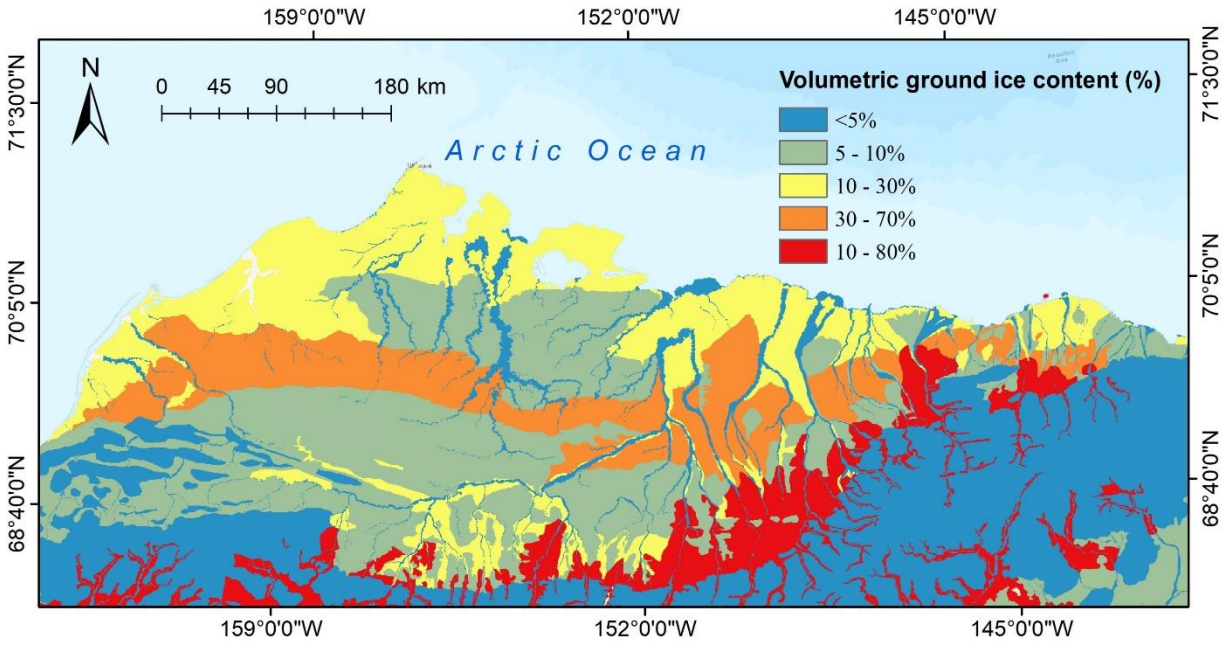

Figure S.1. Ground ice content distribution of North Slope Borough, Alaska (adapted from Jorgenson et al. 2014).

2 Variables used for coastal hazards assessment

ShoreZone is a system that combines aerial imaging, coastal habitat classification, and mapping techniques to inventory the geomorphological and biological attributes of shorelines (Cook et al., 2017). The obtained variables ($R_{Habitats}$, $R_{ShorelineType}$, R_{SLR}) are pre-classified from the data resources. We showed the classification criteria in Tables S.1. and S.2 and the classified results in Figures S.2., S.3., and S.4. The obtained variables (R_{Relief}, R_{Wind}, R_{Waves}, $R_{SurgePotential}$) are ranked based on methods proposed by Gornitz et al. (1990) and Hammar-Klose and Thieler (2001), as shown in Table S.3.

Table S.1. Ranking table of $R_{ShorelineType}$ (Cook et al. 2017).

Shore type exposure	Width	Description
Rock (1)	Wide (>30 m)	Rock Ramp, wide

		Rock Platform, wide
	Narrow (≤30 m)	Rock Cliff
		Rock Ramp, narrow
		Rock Platform, narrow
Rock & sand (2)	Wide (>30 m)	Ramp with gravel beach
		Platform with gravel beach
	Narrow (≤30 m)	Cliff with gravel beach
		Ramp with gravel beach
		Platform with gravel beach
	Wide (>30 m)	Ramp with gravel & sand
		Platform with G & S beach
	Narrow (≤30 m)	Cliff with gravel/sand
		Ramp with gravel/sand
		Platform with gravel/sand
	Wide (>30 m)	Ramp with sand beach
		Platform with sand beach
	Narrow (≤30 m)	Cliff with sand beach
		Ramp with sand beach
		Platform with sand beach
Sand & silt (3)	Wide (>30 m)	Gravel flat, wide
	Narrow (≤30 m)	Gravel beach, narrow
		Gravel flat or fan
	Wide (>30 m)	Sand & gravel flat or fan
	Narrow (≤30 m)	Sand & gravel beach
		Sand & gravel flat or fan
	Wide (>30 m)	Sand beach
		Sand flat
		Mudflat
	Narrow (≤30 m)	Sand beach
Organics, fines, and low vegetated peat (4)	Riparian means organics, fines, low vegetated peat dominate the unit. Current-dominated shore types occur in elongated channels with restricted fetches. Lagoons represent a special coastal feature that has some salt-water influence.	
Permeable human-made structures, glacial, periglacial (permafrost) (5)	Anthropogenic represents permeable human-made structures such as riprap, wooden crib structures and impermeable human-made structures such as concrete seawalls and steel sheet piles. Glacial ice dominates a few places on the Alaska coast. Periglacial represents the inundated tundra or ground ice slumps-dominated segments where thaw-subsidence hazards could occur.	

Geomorphology, which is represented by $R_{\text{ShorelineType}}$, refers to the resistance of coastal areas to inundation and erosion. In this research, we extract geomorphological information from *ShoreZone* database for the coastline of the North Slope Borough. *ShoreZone* provides the classification of the coastline, a polyline layer with 38 geomorphology classes based on lithology and permafrost characteristics. The classification of coastline includes five shore types: gravel; gravel and sand; sand and silt; organics, fines, and low vegetated peat; permeable human-made structures, glacial, and periglacial. In this research, the created polylines are assigned an exposure rank in each 1 km^2 North Slope Borough coastal segment based on the geomorphology classes. The details for

assigning the exposure ranks are listed in Supplementary Table S.1. The spatially distributed shore-type exposure rankings are shown in Figure S.2.

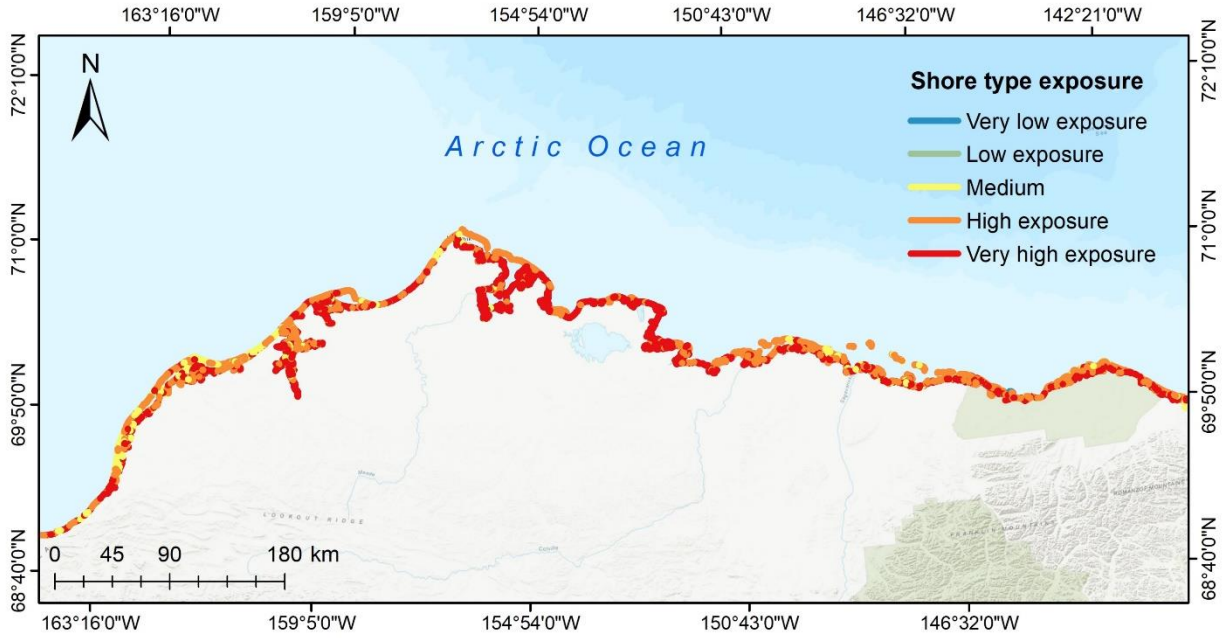

Figure S.2. Example of the shore type exposure provided in the *ShoreZone* database.

Table S.2 Ranking table of $R_{Habitats}$ (Cook et al. 2017).

Habitat classes	Descriptions
Very protected (1)	This category is limited to areas of very low wave exposure and limited diversity of biota, as are seen at the extremely sheltered heads of inlets or in ponded lagoons with a limited intertidal range. Often only the wetland Biobands will be present, and the intertidal is bare of attached biota.
Protected (2)	Attached biota can be patchy due to lack of circulation, although in areas with good circulation, the biobands can be lush. It is indicated by patchy barnacles, Rockweed, and Green Algae Biobands in the intertidal and Eelgrass or sparse Soft Brown Kelps in the subtidal. If the Splash Zone is present, it is narrow (<1 m). Canopy kelps are not usually present. Canopy kelps in otherwise Protected areas can indicate a current dominated Habitat Class.
Semi-protected (3)	The Splash Zone is medium to narrow in width (1-5 m). It is indicated by Barnacle, Rockweed, and Green Algae Biobands which may be lush. In higher SP, Red Algae and Alaria Biobands are often observed. Eelgrass occurs in the lower Semi-Protected areas, and Surfgrass can be found in the higher Semi-Protected areas.

Semi-exposure (4)	The Splash Zone will usually be medium to wide in width (5-10m). This is the exposure category with the highest species diversity. It is indicated by the presence of Dark Brown Kelps, lush Red Algae (especially Coralline Red Algae), Alaria, and in some locations, the Surfgrass Biobands.
Exposure & very exposure (5)	Exposure is used ~~to~~ the wide to very wide Splash Zone (10-20m). The upper intertidal is usually bare-looking, with only a thick Barnacle Bioband visible. The lower intertidal tends to have a lush Dark Brown Kelp Bioband mixed with Red Algae. Nearshore canopy kelp, if present, is Bull Kelp. Very exposure category is used only for areas of extremely high wave energy, where the shoreline is predominantly vertical rock cliff, and there is no moderation of open ocean swells nearshore. The Splash Zone is extremely wide (>20m).

The habitat class represented by R_{Habitats} in *ShoreZone* is a summary attribute that combines both physical and biological characteristics observed for a particular shoreline segment (known as the unit in *ShoreZone*). Habitat information is extracted based on biological characteristics. Biological characteristics refer to typical biota and are classified based on the biota's known wave energy tolerances. *ShoreZone* classifies habitats based on observations of the presence and abundance of biota and wave exposure (coastal orientation, presence of offshore islands, and bathymetry) in each alongshore unit. Consequently, the habitat information of the coastline is divided into five classes: very protected, protected, semi-protected, semi-exposed, and exposed to very exposed. Visualized habitat classes are shown in Supplementary Figure S.3. The detailed classification information can be found in Supplementary Table S.2.

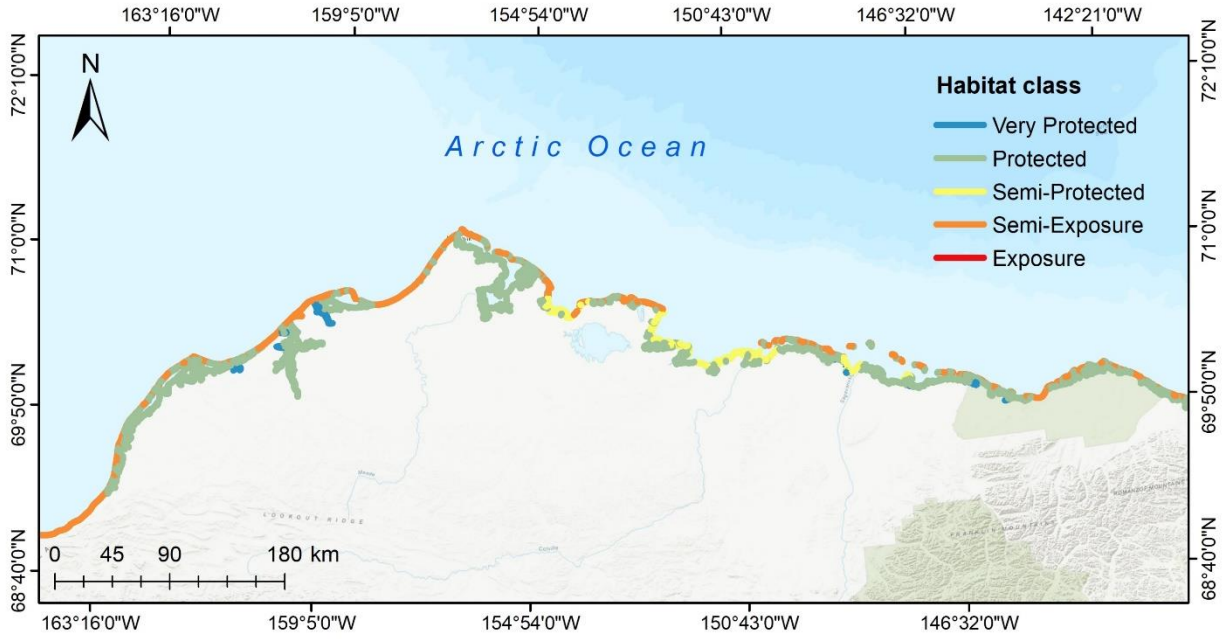

Figure S.3. Examples of the habitat class provided in the *ShoreZone* database.

Table S.3 Ranking table of R_{Relief}, R_{Wind}, R_{Waves}, and $R_{SurgePotential}$ (NCP 2018).

Rank	1 (very low)	2 (low)	3 (moderate)	4 (high)	5 (very high)
Relief	81 to 100 Percentile	61 to 80 Percentile	41 to 60 Percentile	21 to 40 Percentile	0 to 20 Percentile
Wind exposure	0 to 20 Percentile	21 to 40 Percentile	41 to 60 Percentile	61 to 80 Percentile	81 to 100 Percentile
Wave exposure					
Surge potential					

To quantify coastal relief, R_{Relief}, a digital elevation model with a spatial resolution of 5 m, provided by the Polar Geospatial Center (Polar Geospatial Center – Polar Geospatial Center (umn.edu)), is used to generate an elevation rank for each segment, and the average elevation within a radius of 3 km is determined to approximate the variation in coastal relief. For the wind and wave exposure factors, R_{Wind} and R_{Waves}, the highest 10% wind speeds in each of the 16 equiangular sectors are extracted from a compiled eight-year (2008–2016) WAVEWATCH III model dataset (NCP 2018). We adopted wave and wind potential calculations from the InVEST user's guide (Sharp et al. 2014). The details are provided in Supplementary Materials (Eq. S1, S2, S3, and S4). In addition to wind speed and direction, storm surge elevation is related to the time the wind blows. To estimate the surge potential, $R_{SurgePotential}$, the model computes the distance from the segment point to the edge of the continental shelf (NCP 2018). The classification criteria for R_{Relief}, R_{Wind}, R_{Waves}, and $R_{SurgePotential}$ are shown in Table S.3.

The relative exposure to wind and waves is calculated as follows (Sharp et al. 2016):

$$E_{wind} = \sum_{i=1}^{16} U_i P_i F_i \tag{S1}$$

$$E_{wave} = \max(E_w^o, E_w^l) \tag{S2}$$

$$E_w^o = \sum_{i=1}^{16} H[F_i] P_i^o O_i^o \tag{S3}$$

$$E_w^l = \sum_{i=1}^{16} P_i^l O_i^l \tag{S4}$$

where E_{wind} is the wind exposure ($m^2\ s^{-1}$); U_i is the average of the highest 10% wind speed ($m\ s^{-1}$); P_i is the percentage of wind blowing in the *i*-th sector within all wind speed in the record of interest; F_i is the fetch distance (m); E_{wave} is the wave exposure ($kW\ m^{-1}$); E_w^o and E_w^l are oceanic and locally wind-generated wave power, respectively ($kW\ m^{-1}$); $H[F_i]$ is a Heaviside step function of fetch distance; P_i^o and P_i^l are the averages of highest 10% power for respective wave types ($kW\ m^{-1}$); O_i^o and O_i^l are the wave duration for respective wave types (s); *i* is the wind sector.

The current sea-level change, R_{SLR}, is calculated as the increase in water elevation from 1990 to 2023 using tidal gauge data from the National Oceanic and Atmospheric Administration (NOAA) Tides and Currents measurements (NOAA 2023). To assess the variability of coastal hazards in the context of a changing climate, we use the sea level projections under the intermediate low and intermediate high global mean sea level rise (GMSL) scenarios from the NOAA's updated mean projections of sea level rise along the U.S. coastlines (Sweet et al. 2022). The classification information for the sea-level rise scenarios is shown in Figure S.4.

The sea-level rise (SLR) scenarios and air temperature warming scenarios are related. The SLR scenarios in this study were adapted from Sweet et al. (2020). Sweet et al. (2020) built these SLR scenarios by using a variety of different resources (Kopp et al. 2014) to generate distributions of future global and regional sea level changes consistent with low (RCP2.5), medium (RCP4.5), and high (RCP8.5) emissions forcing. These resources include global climate model (GCM) projections, the IPCC AR5 assessment of ice-sheet changes, and structured expert-judgment ice-sheet projections.

In particular, the GCMs of the fifth phase of the Coupled Model Intercomparison Project (CMIP5) were used for projecting causes of global mean sea level rise, i.e., thermal expansion, ocean dynamics, glaciers and ice caps (Sweet et al. 2017). The five GCMs – NCAR-CCSM4, GFDL-CM3, GISS-E2R, IPSL-CM5A-LR, and MRI-CGCM3 – that we used for air temperature dynamics projections are all included in the GCMs of CMIP5 for SLR projections. For detailed CMIP5 models used for SLR projections, please refer to Appendix D. of Sweet et al. (2017).

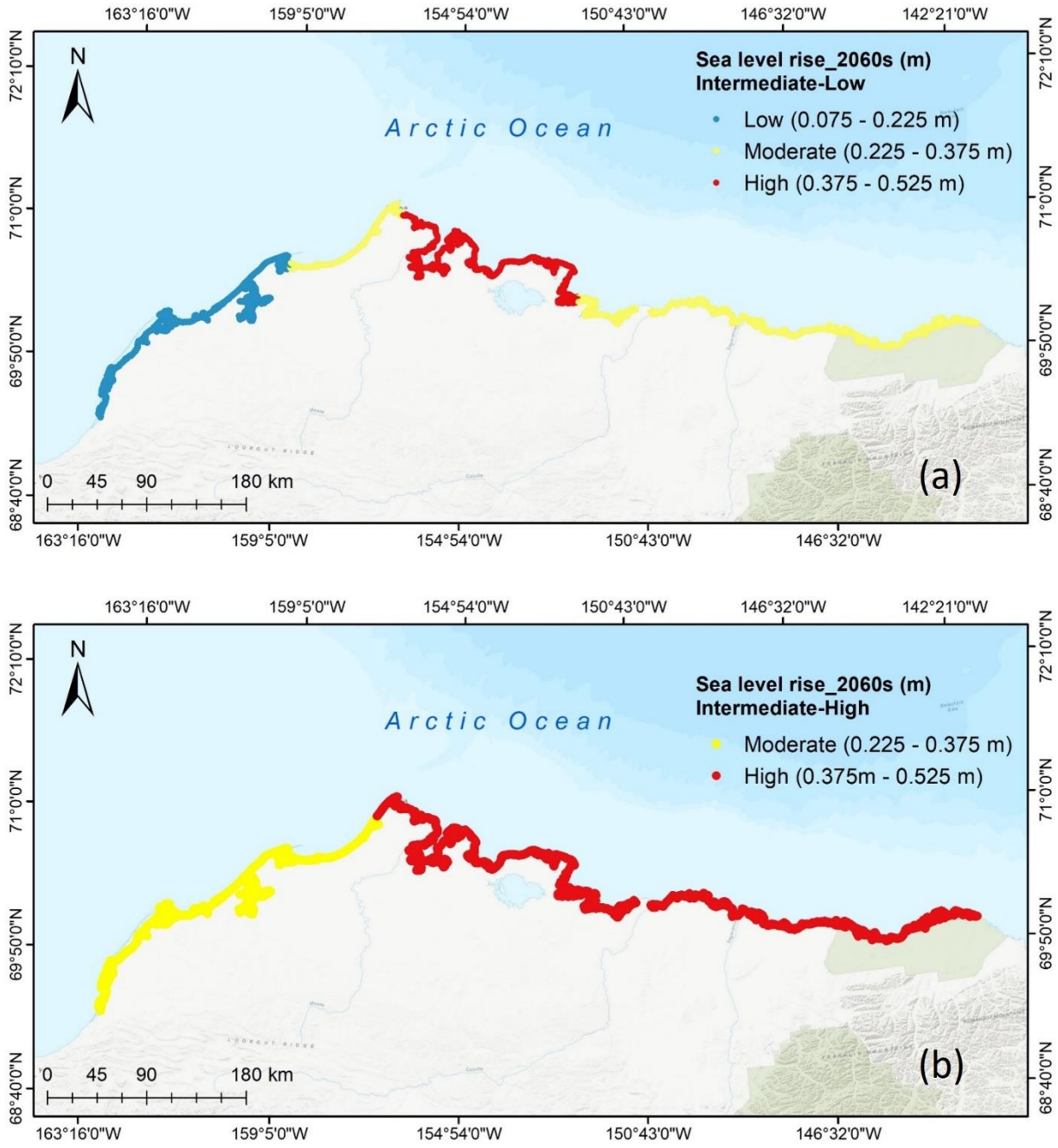

Figure S.4. Distributions of sea level rise R_{SLR} along the coast of the North Slope Borough under the current (2020s) and future (2060s) scenarios (Intermediate-Low and Intermediate-High).

3 Future conditions of permafrost

The ground thermal properties used in the GIPL-2.0 model were established based on soil texture and vegetation cover. The landscape database by Jorgenson et al. (2014) and an ecological map by

Jorgenson and Heiner (2003) were used to parameterize the soil texture and vegetation type. Air temperature dynamics were defined by using the monthly averaged data sets complied by the Scenarios Network for Alaska and Arctic Planning group (SNAP). In particular, we deployed a monthly averaged Climate Research Unit (CRU) TS3.1 data set (Harris et al. 2014) downscaled by SNAP to a 770m resolution using the delta method (Hijmans et al. 2005). For the future modeling runs with the RCP 4.5 and 8.5 forcing, we used an average composed of downscaled monthly averaged outputs of five general circulation models (NCAR-CCSM4, GFDL-CM3, GISS-E2R, IPSL-CM5A-LR, and MRI-CGCM3) (Nicolsky et al. 2017).

Figure S.5 shows the MAGT at a depth of 1m below the ground surface and ALT projected for the North Slope Borough for the periods 2020-2029 and 2060-2069 under RCP4.5 and for the period of 2060-2069 under RCP8.5. Figure S.5a, c, e depict the MAGT modeling results, while Figure S.5b, d, and f show the ALT modeling results. Figure S.6 shows the taliks thickness projected by GIPL-2.0 for the period of 2060-2069 using RCP4.5 and RCP8.5.

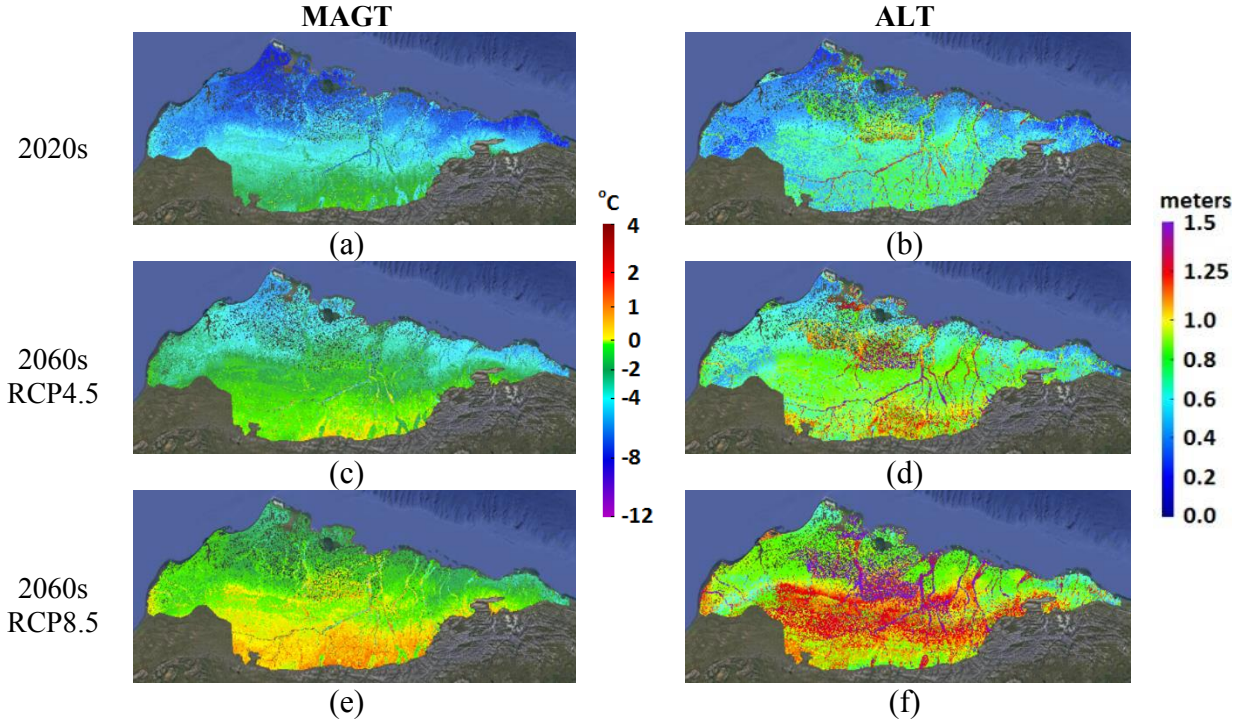

Figure S.5. Current (year 2020s) and projected (year 2060s under RCP4.5 and RCP8.5) mean annual ground temperature (MAGT) at 1 m below ground surface and ALT of North Slope Borough, Alaska. The MAGT and ALT are simulated using climate forcing from Global Climate Models. The figures are adopted from Nicolsky et al. (2017). Nicolsky et al (2016) John Wiley & Sons. ©2016. American Geophysical Union. All Rights Reserved.

Figure S.6. Projected (year 2060s under RCP4.5 and RCP8.5) taliks thickness. The figures are adopted from Nicolsky et al. (2017). Nicolsky et al (2016) John Wiley & Sons. ©2016. American Geophysical Union. All Rights Reserved.

4 Permafrost thaw potential (PTP)

R_{PTP} is derived from index-based permafrost thaw hazard maps with a spatial resolution of 1 km. Raster maps of the potential thaw settlement are used to calculate the PTP of each 1 km^2 shoreline area (i.e., the segment point). The five-class thaw subsidence hazard maps are first given a ranked number of 1, 2, 3, 4, or 5 representing low to high hazard potential. We calculate the average PTP within a radius of 3 km to decrease the uncertainty. The average PTP is then assigned to the nearest segment point to represent the shoreline PTP. In Figure S.7., we show the gridded shoreline PTP of North Slope Borough, Alaska.

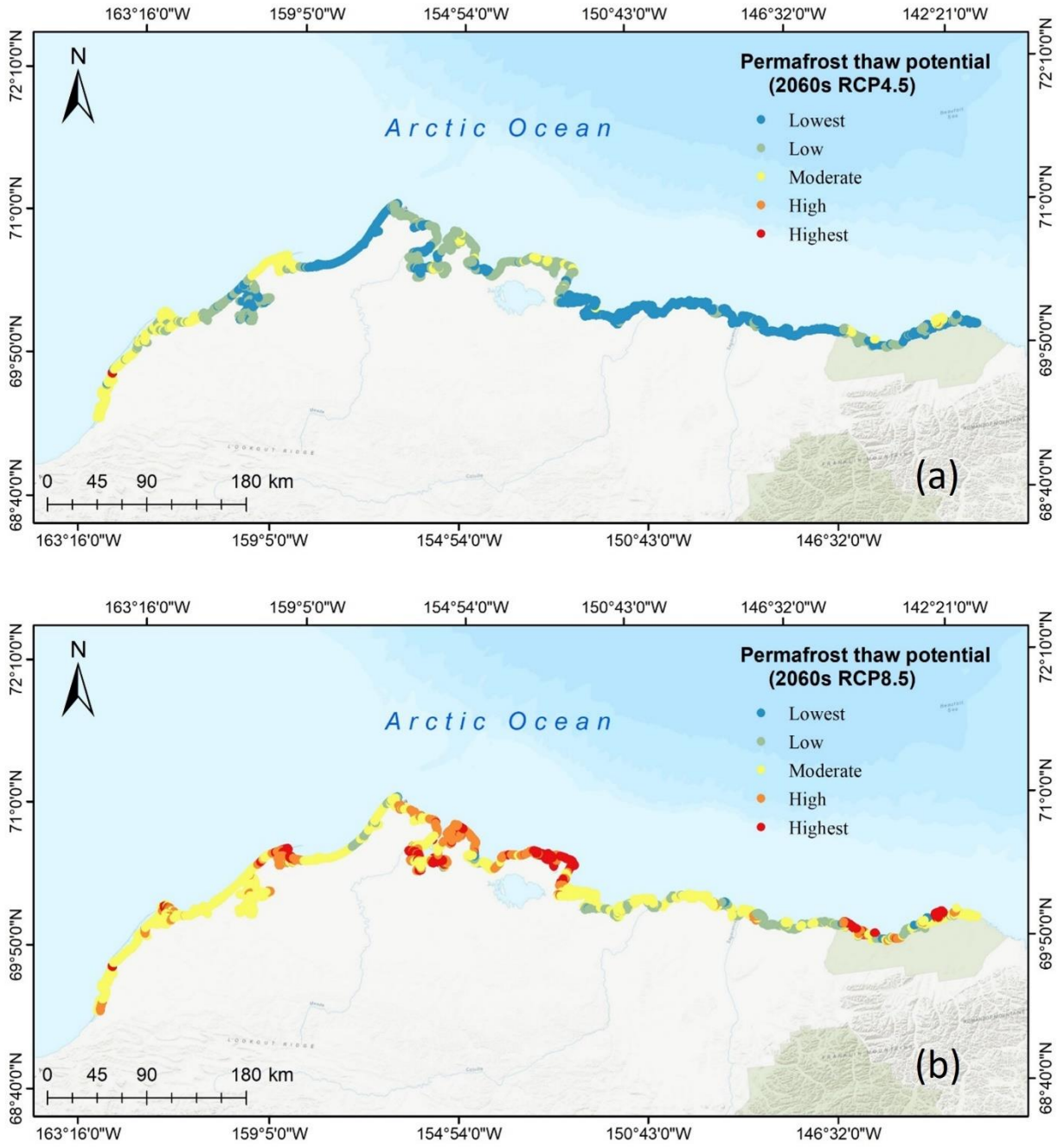

Figure S.7. Gridded shoreline PTP of North Slope Borough, Alaska. (a) under RCP4.5 scenario; (b) under RCP8.5 scenario.

References

Cook, S., Daley, S., Morrow, K., Ward, S., 2017. ShoreZone Coastal Imaging and Habitat Mapping Protocol. Report Prepared by Coastal and Ocean Resources, Victoria, bc, Canada.

Gornitz, V., 1990. Vulnerability of the East Coast, USA to future sea level rise. *Journal of Coastal research, pp*.201-237.

Hammar-Klose, E.S. and Thieler, E.R., 2001. Coastal vulnerability to sea-level rise: a preliminary database for the US Atlantic, Pacific, and Gulf of Mexico coasts (No. 68). *US Geological Survey.*

Harris, I.P.D.J., Jones, P.D., Osborn, T.J. and Lister, D.H., 2014. Updated high‐resolution grids of monthly climatic observations–the CRU TS3. 10 Dataset. *International journal of climatology, 34*(3), pp.623-642.

Hijmans, R.J., Cameron, S.E., Parra, J.L., Jones, P.G. and Jarvis, A., 2005. Very high resolution interpolated climate surfaces for global land areas. *International Journal of Climatology: A Journal of the Royal Meteorological Society, 25*(15), pp.1965-1978.

Jorgenson, M.T. and Heiner, M., 2003. Ecosystems of northern Alaska. Anchorage, Alaska: The Nature Conservancy.

Jorgenson, M.T., Kanevskiy, M., Shur, Y., Grunblatt, J., Ping, C.L. and Michaelson, G., 2014. *Permafrost database development, characterization, and mapping for northern Alaska*.

Kopp, R.E., Horton, R.M., Little, C.M., Mitrovica, J.X., Oppenheimer, M., Rasmussen, D.J., Strauss, B.H. and Tebaldi, C., 2014. Probabilistic 21st and 22nd century sea‐level projections at a global network of tide‐gauge sites. Earth's future, 2(8), pp.383-406.

NCP., 2018. Natural Capital Project: InVEST Version 3.5.0 Sample Datasets. http://data.naturalcapitalproject.org/invest-data. Accessed: 112-10-20182023.

Nicolsky, D.J., Romanovsky, V.E., Panda, S.K., Marchenko, S.S. and Muskett, R.R., 2017. Applicability of the ecosystem type approach to model permafrost dynamics across the Alaska North Slope. *Journal of Geophysical Research: Earth Surface*, *122*(1), pp.50-75.

Sharp, R., Tallis, H.T., Ricketts, T., Guerry, A.D., Wood, S.A., Chaplin-Kramer, R., Nelson, E., Ennaanay, D., Wolny, S., Olwero, N. and Vigerstol, K., 2014. InVEST user's guide. *The Natural Capital Project: Stanford, CA, USA*.

Sweet, W.V., Hamlington, B.D., Kopp, R.E., Weaver, C.P., Barnard, P.L., Bekaert, D., Brooks, W., Craghan, M., Dusek, G., Frederikse, T. and Garner, G., 2022. *Global and regional sea level rise scenarios for the United States: updated mean projections and extreme water level probabilities along US coastlines*. National Oceanic and Atmospheric Administration.

Sweet, W.V., Kopp, R.E., Weaver, C.P., Obeysekera, J., Horton, R.M., Thieler, E.R. and Zervas, C., 2017. Global and regional sea level rise scenarios for the United States (No. CO-OPS 083).